2019 IEEE Intelligent Transportation Systems Conference (ITSC)
Auckland, NZ, October 27-30, 2019

Safety Criteria Analysis for Negotiating Blind Corners in Personal Mobility Vehicles Based on Driver's Attention Simulation on 3D Map

Naoki Akai[1], Takatsugu Hirayama[2], Luis Yoichi Morales[2], and Hiroshi Murase[1]

***Abstract*— In this study, we attempt to establish the numerical safety criteria for negotiating blind corners in personal mobility vehicles (PMVs). Safety should be the most important consideration in designing autonomous PMVs. However, determining the suitable trade-off between safety and speed is a weighty concern because speed is significantly compromised when performing overly safe navigation. We analyze the driving behavior of a robotic PMV operated by a human driver. The robotic PMV can measure the driver's gaze, and allows us to recognize both the pose of the PMV and the driver's visual attention on a 3D map. As a result, the occluded areas for the driver can be estimated. Then, potential colliding hazard obstacles (PCHOs) are simulated based on the occlusion. PCHOs refer to occluded obstacles that the driver encounters suddenly with which he cannot avoid collision. The participants of our experiments were one skillful and three non-skilled ones. Experimental results demonstrate that similar PCHOs are observed even when the driving styles of the participants are different. Additionally, the existence of a boundary that distinguishes expected and unexpected obstacles is indicated by investigating the parameters of the PCHOs. Finally, we conclude that the boundary could be utilized as a numerical criterion for ensuring safety while negotiating blind corners.**

I. Introduction

There is a trade-off relationship between safety and speed in path and motion planning problems for the autonomous navigation of personal mobility vehicles (PMVs). Although safety should be the paramount consideration, speed and smoothness are significantly compromised when performing overly safe navigation. However, determining the suitable trade-off parameters of these factors is challenging, because it is difficult to numerically recognize the criteria for ensuring safety. In this study, we attempt to indicate the numerical safety criteria for PMVs negotiating blind corners.

Although humans can determine reasonable trade-off parameters based on personal experiences, there could be potential colliding hazard obstacles (PCHOs) even when blind corners are carefully navigated because of the occlusion. "PCHOs" refer to obstacles that suddenly appear from the occlusion, with which it is impossible to avoid collision. Nevertheless, drivers do not be overly conscious to the PCHOs because smoothly negotiating blind corners is equally desirable. Our conjecture is that humans empirically have a boundary that divides expected and unexpected obstacles when negotiating blind corners, and such a boundary could be utilized to establish the numerical criteria for ensuring safety. This work determines this boundary by observing the attention of drivers on a three-dimensional (3D) map.

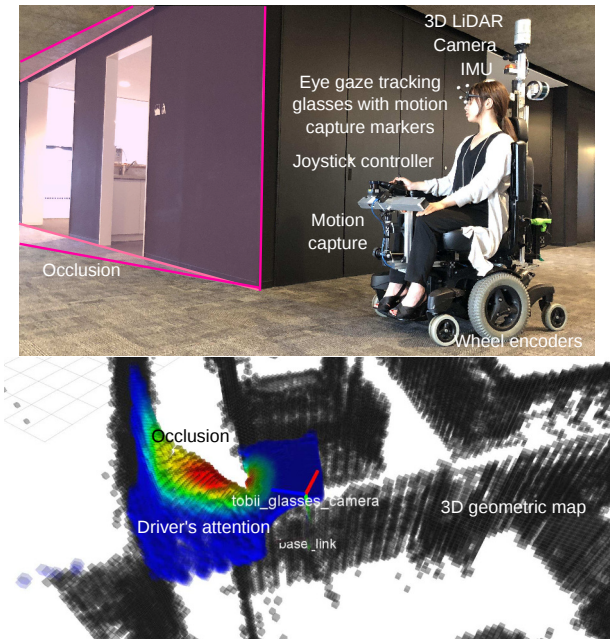

Fig. 1. 3D attention simulation with the robotic PMV (top) and a visualization sample of the simulated driver's visual attention on the 3D map (bottom). Dead angle areas are estimated, and PCHOs are simulated.

We developed a wheelchair-based robotic PMV for this work. The PMV can measure the driver's gaze, enabling us to recognize both the pose of the PMV and the driver's gaze on the 3D map. We simulate the driver's visual attention on the 3D map using this information. Figure 1 shows the PMV (top) and a visualization example of the simulated driver's visual attention prior to negotiating a blind corner (bottom). The occluded areas for the driver are estimated on the 3D map. Based on the occluded areas, we also simulated PCHOs to investigate unexpected obstacles. The participants of the experiments were one skilled and three unskilled drivers. Experimental results show that similar PCHOs are observed by all the participants despite the differences in driving style. Additionally, investigating the parameters of the PCHOs indicates the existence of a boundary between the expected and unexpected parameters of the PCHOs. Finally, we concluded that this boundary can be utilized as a numerical boundary for ensuring safety for PMVs negotiating blind corners.

[1]Naoki Akai and Hiroshi Murase are with the Graduate School of Informatics, Nagoya University, Nagoya 464-8603, Japan {akai, murase}@nagoya-u.jp

[2]Takatsugu Hirayama and Luis Yoichi Morales are with the Institute of Innovation for Future Society (MIRAI), Nagoya University, Nagoya 464-8601, Japan morales_yoichi@coi.nagoya-u.ac.jp, takatsugu.hirayama@nagoya-u.jp

The contributions of this work are twofold:

- We developed methods to simulate driver's attention and PCHOs on the 3D map.
- Numerical criteria that could distinguish expected and unexpected obstacles and could be utilized as a numerical boundary for ensuring safety in blind corners is designed.

The rest of this paper is organized as follows. Section II provides an overview of related works. Section III describes the robotic PMV and the method for analyzing the driver's visual attention. Section IV details the experimental procedure, and presents the results. Section V is the conclusion.

II. Related works

This section briefly summarizes works related to path and motion planning around blind corners and the analysis of the driver's gaze.

A. Path and motion planning around blind corners

The majority of path and motion planning studies are preoccupied with determining the path or motion sequence that allows robots to quickly arrive at a destination without collision; an example of such research endeavors is [1]. It is, however, not easy to develop a perfect solution, because there is a trade-off relationship between safety and speed. In recent years, many studies have explored various factors toward determining the solution, e.g., [2]. Although, there are many factors that enable advanced navigation of PMVs, a more complex trade-off dynamic will emerge. Unfortunately, it is necessary to manually adjust the trade-off parameters, which is a time-consuming task.

Some authors have proposed autonomous navigation methods that prioritize the riding comfortability of the passenger in a wheelchair as a means of ensuring safety. Morales *et al*. posited that visibility and comfortability are related, and proposed a path planning method that computes visibility using a 3D LiDAR [3]. Sawabe *et al*. proposed a velocity control method based on visibility, and confirmed that the proposed control method could lower passengers' stress [4]. Additionally, they analyzed passenger stress characteristics with different stress factors using two physiological indices, heart rate and galvanic skin response sensors, during the usage of autonomous wheelchairs [5]. These works demonstrated that suitable path planning and velocity declaration are useful for improving ride comfortability. However, their methods do not take the driver's visual attention into consideration when determining the trade-off parameters.

In the field of intelligent vehicles, similar researches have been conducted on visibility by several authors. Takeuchi *et al*. proposed a traffic prediction method using a high definition map [6]. In the method, obstacles that may spring out from blind corners are modeled using a particle filtering algorithm, and the linear velocity of the obstacles are estimated. Muffert *et al*. presented a warning system using stereo vision-based obstacle detection for supporting the negotiation of roundabouts [7]. Hörmann *et al*. proposed a safe strategy for automated left-turn maneuvers in a case where the field of view is partially occluded [8]. Using sensor measurements, these works estimate the states of obstacles that may potentially collide with an ego-vehicle; however, data are not acquired from humans.

A previous study by our group, Morales *et al*., analyzed the behavior of cars driven by skillful drivers negotiating blind corners, and modeled the velocities of the moving obstacles that may spring out from the corner [9]. Yoshihara *et al*. proposed a planning method that uses a model to determine the suitable velocity deceleration [10]. In [9], the parameters of the obstacles were determined based on the trajectory and velocity profiles estimated by the 3D localization method presented in [11], [12]. In these works, the attention of the drivers was not fully taken into consideration during obstacle modeling.

Learning-based methods, such as inverse reinforcement learning and end-to-end navigation, can be used to simulate the driving styles of skillful drivers [13]–[16]. These methods basically receive the sequence of behavior or raw sensor measurements, and learn the relationships between the input data and driving styles. Hence, these methods do not explicitly take the driver's visual attention into consideration.

B. Analysis of driver's gaze

Because there is a significant link between the driver's gaze and driving behavior, many authors have analyzed driver's gaze [17], [18].

In [19], [20], convenient methods that do not use glasses to track the driver's gaze were presented. In [20], their system is evaluated on a dataset collected from natural on-road driving in urban streets and freeways. Doshi *et al*. analyzed the significance of the driver's gaze during driving [21]. They also created a saliency map based on the surrounding traffic characteristics of the ego-vehicle, and demonstrated the capability of the proposed methodology to improve driver attention and behavior, as well as intent prediction. However, they do not analyze the driver's visual attention in a 3D geometric space, because a 3D geometric map was not available in their work.

Miyajima *et al*. analyzed the relationship between the drivers' gaze and negative adaptation to automated driving, i.e., trusting too much in the automated car's ability [22]. This approach attempts to extract characteristics related to negative adaptation by analyzing the driver's gaze. On the other hand, the approach presented in this work attempts to extract the criteria for efficient autonomous navigation by analyzing the gaze.

In [23], [24], Hirayama *et al*. posited that drivers of ego-vehicles naturally look at cars that will overtake them; they analyzed the temporal relationships between the driver's gaze and the surrounding vehicle behaviors for detecting the driver's distraction. In these methods, the surrounding situation of the ego-vehicle was measured using only on-board sensors because map information was not available.

Some authors have presented 3D attention visualization and gaze tracking methods [25], [26]. In these approaches, camera- or RGB-D-camera-based SLAM methods, such as

those presented in [27], [28] were used to build 3D maps. Rhinehart *et al*. proposed an activity-forecasting method based on inverse reinforcement learning using a first-person video sequence [29] by extending the work presented in [30]. In our approach, we use a 3D geometric map and a localization method for estimating the driver's gaze, and the gaze, as projected on the 3D map, is utilized for analyzing potential hazards for the driver.

III. Simulation of Driver's Visual Attention and Potential Colliding Hazard Obstacles

A. Wheelchair-based robotic PMV

Top of the Fig. 1 shows the developed wheelchair-based robotic PMV that allows us to recognize driver's eye-gaze on a 3D map. The PMV is equipped with wheel encoders, a 3D LiDAR, and an IMU to build a 3D map, and to localize its own pose on the map. The PMV is also equipped with a driver-facing motion capture system[1]. The driver wears eye-gaze tracking glasses[2]. Motion capture markers are attached to the glasses, and the motion capture system tracks the markers. Because the motion capture system tracks the markers, we calibrate a rigid body composed of the markers and a camera attached to the glasses (eye-tracking camera). All of the measurement devices are calibrated off-line, i.e., transformation matrices between the devices are available[3]. Finally, the PMV performs the localization, and the direction of the driver's gaze can be obtained on the 3D map.

B. Simulation of driver's visual attention

To simulate the driver's visual attention on the 3D map, as shown in the Fig. 1, we first build a 3D map of the target environment. Because we conducted the experiments indoors, a 2D SLAM method presented in [31] is first used for building a consistent 2D map. The 3D map is built by plotting the point cloud obtained using the 3D LiDAR according to the trajectory estimation conducted with the 2D SLAM. To efficiently handle the 3D map, the OctoMap presented in [32] is used. The method presented in [33] is used for localizing the pose of the PMV.

To simulate the driver's visual attention, we first obtain the pose of the eye-tracking camera and the gaze direction on the 3D map frame. We then perform ray casting on the 3D map around the eye-gaze direction, and obtain the hitpoints on the 3D map as a point cloud. The unmapped obstacles measured by the 3D LiDAR are added to the OctoMap before ray casting. Bottom of the Fig. 1 shows a visualization example of the simulated driver's visual attention. Based on [34], the raycasting horizontal and vertical angles were respectively set to 90 and 60 degrees. The resolution of the ray-casting angle was set to 1 degree. This attention simulation is performed according to the measurement cycle of the 3D LiDAR, i.e., 10 Hz. Finally, we obtain the occluded areas for the driver through the attention simulation.

[1] https://optitrack.com/products/v120-trio/, accessed at 8 April 2019.

[2] https://www.tobiipro.com/product-listing/tobii-pro-glasses-2/, accessed at 8 April 2019.

[3] Calibration between the measurement devices were manually done.

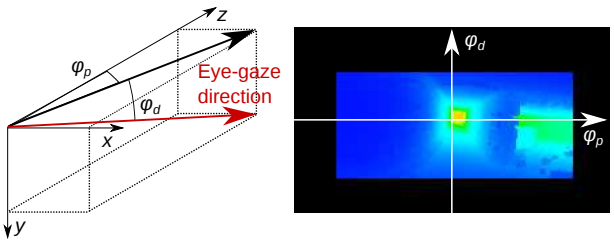

Fig. 2. Coordinates of the eye-tracking camera (left) and an example of the depth map built on the basis of the simulated driver's attention (right). Red and blue denote long and short distances.

C. Obstacle visibility check

We check the visibility of the obstacles that may be candidates of PCHOs. We assume that obstacles exist all of free spaces where objects can exist. To check the visibility, we first build a depth map in the eye-tracking camera frame using the point cloud obtained via attention simulation. Figure 2 illustrates the coordinates of the eye-tracking camera, and provides an example of the depth map. The origin and horizontal and vertical axes of the depth map are respectively the origin of the eye-tracking camera and pitch angle of the eye-gaze direction, φ_p, and angle between the eye-gaze direction and the xz-plane, φ_d.

We assume that the shape of the obstacles is approximately represented by a cylinder, and the height, h, and diameter, d, are regarded as their parameters. Several points of the obstacle in the map frame, $\mathbf{p}_o^m$, are transformed into the eye-tracking camera frame; they are denoted by $\mathbf{p}_o^c = {}^c T_m \mathbf{p}_o^m$. Where ${}^cT_m$ is a transformation matrix from the map frame to the eye-tracking camera frame, and $\mathbf{p}_o^c$ is the obstacle point in the eye-tracking camera frame. If the distance of the depth map related to $\mathbf{p}_o^c$, d_i, is shorter than the distance between the eye-tracking camera and the obstacle, $d_i < ||\mathbf{p}_o^m - \mathbf{x}^c||_2$, the obstacle is categorized as invisible, i.e., it is located in the occluded areas. Where $\mathbf{x}^c$ is the eye-tracking camera's pose in the map frame and $||\cdot||_2$ is an operator of the $l2$-norm.

In experiments, the obstacle parameters, h and d, were set to 1.8 m and 0.6 m. An obstacle is categorized as visible based on 14 points; the obstacle is categorized as invisible if all the points are invisible.

D. Simulation of PCHOs

Obstacles categorized as invisible are treated as candidates of PCHOs and possibility of collision with the PMV is simulated. Figure 3 demonstrates how to simulate the parameters of the PCHOs. We first predict pose of the PMV if the PMV does immediate stop as:

$$\begin{aligned} t^{'} &= t_f + t_b, \\ d^{'} &= d_f + d_b, \\ d_f &= v_t t_f, \\ t_b &= v_t/(\mu g), \\ d_b &= v_t^2/(2\mu g), \end{aligned} \tag{1}$$

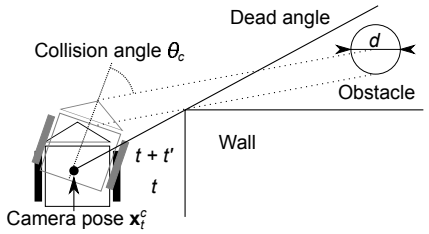

Fig. 3. Simulation of potential colliding hazards

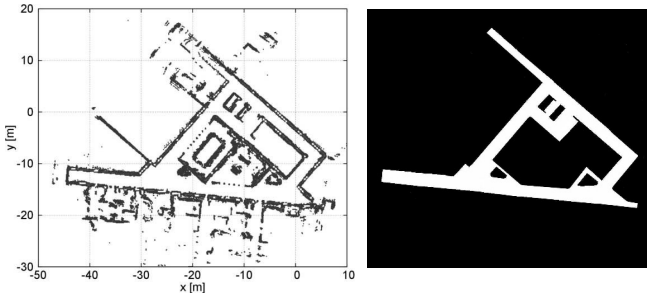

Fig. 4. Environment maps. (left) geometric map (right) free space map. It should be noted that the geometric map has height information (3D points).

where t_f and d_f are free running time and distance, t_b and d_b are braking time and distance, v_t is the current linear velocity of the PMV, and μ and g are the friction coefficient and gravitational acceleration, respectively. In this work, static parameters, t_f, μ, and g, were set as $t_f = 0.5$ s, $\mu = 0.9$, and $g = 9.8\ \mathrm{m/s^2}$. By using $t^{'}$ and $d^{'}$, the PMV's pose after time $t^{'}$ is predicted.

Then, the possibility of the PMV colliding with the invisible obstacles is computed. We assume that the obstacles linearly move towards the front of the PMV. The obstacles that can make it to the front of the PMV without colliding with the objects located in the 3D map are detected as the PCHOs. We compute the linear velocity, v_o, and the collision angle, θ_c, of the PCHOs, and these parameters are used for analyzing driving behavior. The linear velocity of the obstacles is computed by dividing the distance from the front of the PMV to the obstacle by $t^{'}$.

IV. Experiments

A. Experimental environment

We conducted the experiments in an indoor office-like environment. Figure 4 shows the 3D (left) and free space (right) maps of the environment. The 3D map is used for localizing the pose of the PMV, and simulating the driver's visual attention. The white color represents the free space, and is used for simulating the PCHOs.

B. Condition of participants

The participants are one skillful and three non-skilled drivers. A *skillful driver* (SD) is a person who drives the PMV often. A *non-skilled driver* (NSD) is a person who is not used to driving the PMV. The participants are familiar with the environment because they work in the environment. Additionally, all the participants have a Japanese driving license, i.e., they passed the vision test required for the license. The gender-age of the SD, NSD1, NSD2, and NSD3 are male-28, male-40, female-40, and female-41, respectively. Before the experiments, the following instruction was given to the participants: "Please carefully drive the PMV while confirming safety with your eyes."

C. Results by the skillful driver

We first analyzed the driving of the SD. Figure 5 shows the analysis results in the clockwise (CW) direction. The top figure shows the estimated trajectory of the eye-tracking camera; the colored portions represent the PMV's linear velocity and eye-gaze behavior. The bottom figure shows the PCHOs. It should be noted that there were several PCHOs in each computation cycle (10 Hz); however, we selected the PCHO with the slowest linear velocity for easy analysis. Figure 6 enlarges the area A, shown in the Fig. 5. In Fig. 3, the size and color of the circles represent the linear velocity of the PCHOs, v_o, and collision angle, θ_c, shown. The radius of the circles is denoted as $v_o/25$ m.

Additionally, the top of Fig. 7 shows the eye-gaze angles in the 3D LiDAR frame during negotiation of the blind corner shown in Fig. 6. These angles are denoted as:

$$\begin{aligned} \mathrm{Yaw} &= -\tan^{-1}(y^l/x^l), \\ \mathrm{Pitch} &= \tan^{-1}(z^l/x^l), \end{aligned} \tag{2}$$

where $\mathbf{p}^l = (x^l, y^l, z^l)$ is a hit point of the eye-gaze direction with the 3D map in the 3D LiDAR frame. Positive regions of Yaw and Pitch angles represent right and top sides, respectively. These angles consider translational and rotational movements of the eye-tracking camera and are differ from angles shown in the Fig. 2. These results indicate that although the SD carefully checked both the left and right sides, there were PCHOs. However, these PCHOs are regarded as non-realistic obstacles because they have non-realistic parameters. For example, the PCHOs that have the potential to collide with the PMV from the front have significantly fast velocity, typically over $30\ \mathrm{m/s}$. On the other hand, it is considered an accident for the SD, if there is a side collision with the PCHOs, or if the PCHOs have a large collision angle, or do not have large velocity. We therefore regarded these PCHOs as unexpected obstacles for the SD.

D. Results by the non-skilled drivers

We then analyzed the driving of the NSDs in the CW direction. Top figures of the Fig. 8 show the estimated trajectories of the eye-tracking camera and eye-gaze behaviors. Figure 7 also shows the eye-gaze angles of the NSDs as they negotiate the blind corner shown in Fig. 8. As can be seen from these figures, driving and eye-gaze behaviors of each driver was unique. In particular, the variance of the eye-gaze angles of the NSD2 was obviously smaller than that of the other drivers. Nevertheless, similar PCHOs were observed in their results. Additionally, the parameters of the PCHOs are also non-realistic, as described in IV-C.

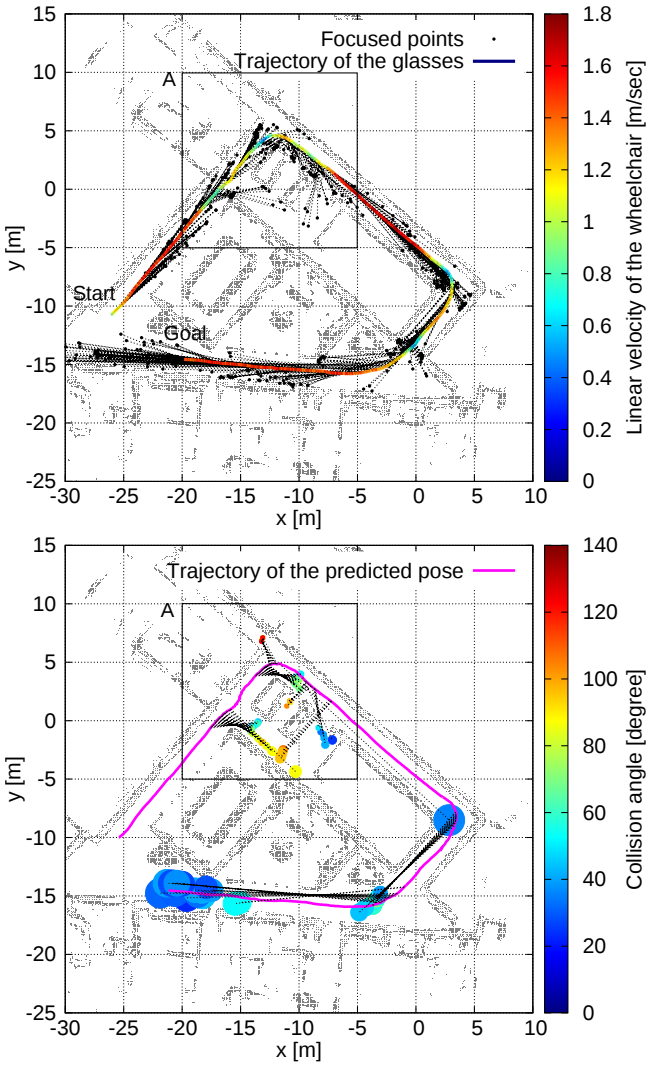

Fig. 5. SD's results in CW direction. The top figure shows the estimated trajectory of the eye-tracking camera and indicates the driver's focus of attention. The dashed lines depict the gaze direction of the driver. The bottom figure shows the predicted poses of the PMV and the PCHOs. The size and color of the circles depict the linear velocity of the PCHOs and the collision angle shown in Fig. 3. The dashed lines shown in the bottom depict the possible paths of the PCHOs.

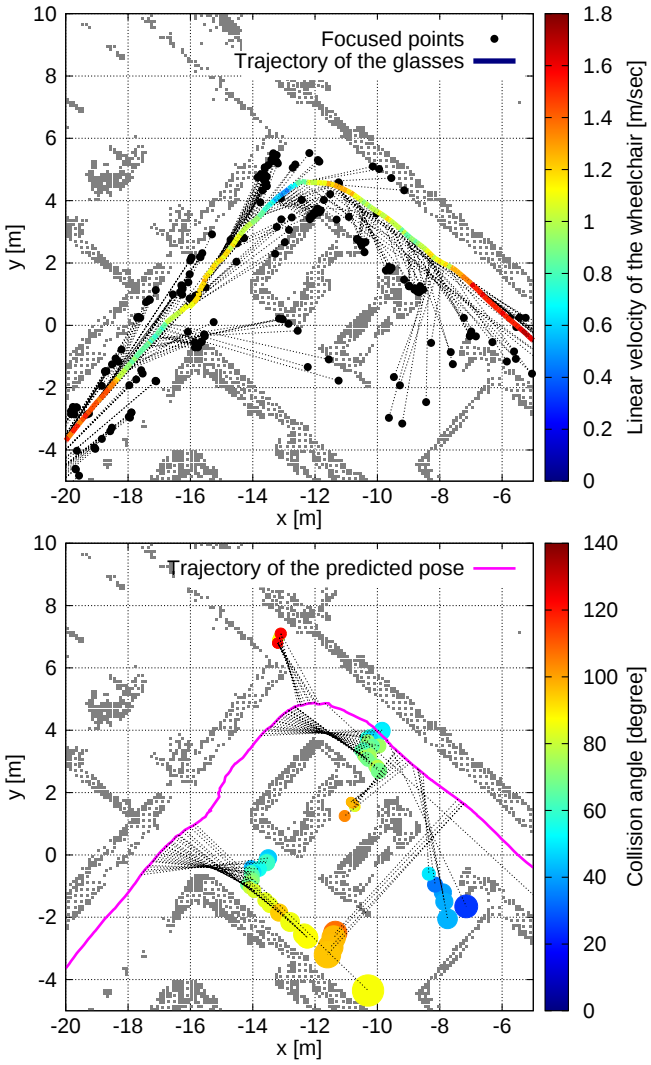

Fig. 6. Enlarged figures of the area A, shown in Fig. 5.

As we mentioned in III-C, perception simulation for PCHOs was performed using the depth map built on the basis of the simulated driver's attention. In the perception simulation, we did not consider the performance differences of central and peripheral visions. Additionally, we assumed that the drivers can perceive all the occluded obstacles, if they locate the field of view, and all the drivers have the same perception ability. These assumptions may be considered as the reason why similar PCHOs were observed. Therefore, we discuss the validity of the experiments using these assumptions in IV-F.

E. Safety criteria

Figure 10 shows the relationship between the collision angle and linear velocity of the PCHOs obtained across all the experiments. This figure also includes the CCW direction results; each participant drove thrice in both the CW and CCW directions. Figure 9 shows examples of the results obtained for the CCW driving in the area A. The Fig. 10 shows that there is a boundary, drawn with the black line.

As abovementioned, the PCHOs are regarded as unexpected obstacles for the drivers. We therefore consider that the upper region of the boundary indicates the set of unexpected obstacles during driving, and the PCHOs included in the area should be ignored to realize human-like autonomous navigation. Moreover, it is necessary for the PMVs to perform path and motion planning that recognizes the PCHOs that do not appear in the bottom areas of the boundary. Such planning will closely mirror human planning that as it efficiently ignores unexpected obstacles. Finally, we conclude that the boundary could be used as numerical criteria for ensuring safety in PMVs' autonomous navigation.

F. Discussion

We assumed that all the participants possess equal visual perception ability. We also ignored the performance differ-

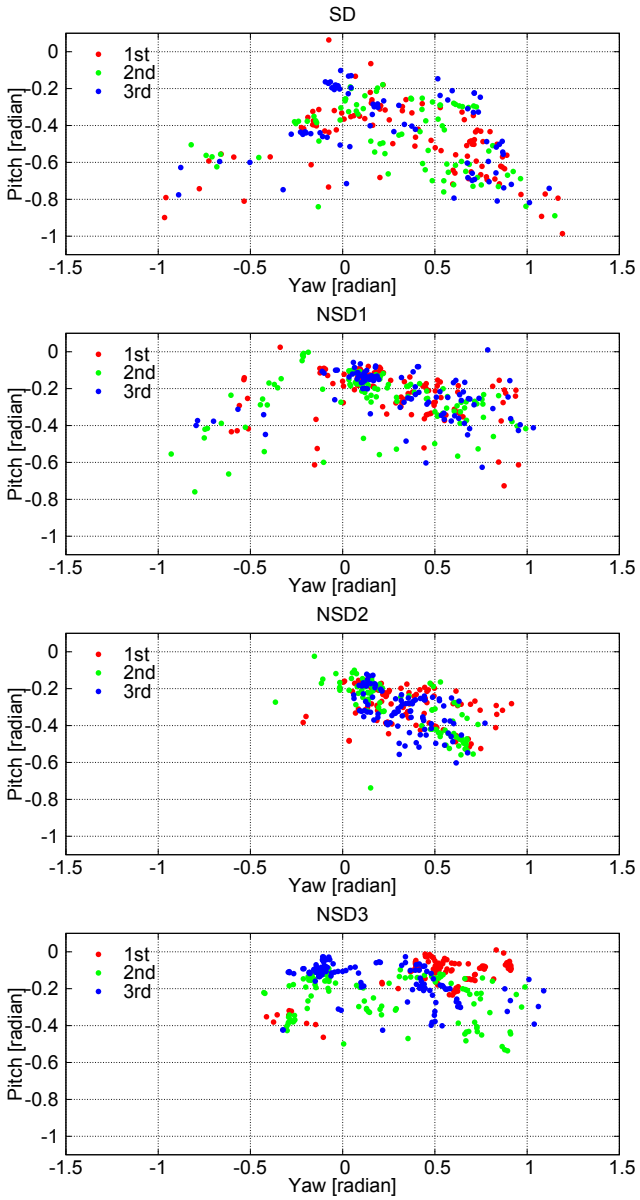

Fig. 7. Gaze angles in the 3D LiDAR frame during negotiation of the blind corner shown in Figs. 6 and 8.

ences of the central and peripheral visions. However, the different performances of these visions have been presented [35], [36]. These assumptions are not suitable for exact analysis, however the modeling of the human's detection and perception ability is a significant task [37]. Hence, we briefly discuss the validity of the perception model used in this work.

Many studies related to the visual function of overlooking in traffic situations mainly focus on the object detection ability, e.g., [38]. The ability to detect the movement of objects in peripheral vision is considered an important factor for ensuring the driver's safety [39], [40]. The role of the peripheral vision in detecting relative movement is the participant of a recent research [41]. These works showed that the peripheral vision can efficiently detect moving objects.

It is well known that habituation is useful for improving skills [42]. Because the environment is familiar to the participants, they could quickly discern changes in the environment. Furthermore, as previously stated, we had told the participants to carefully drive the PMV while confirming safety with their eyes. This information could be regarded as a pre-cue that makes the participants alert to obstacles. The effectiveness of the pre-cue in enabling the participants to quickly respond to the target stimulus was shown [43]. Hence, it could be surmised that the participants quickly detected moving objects even when they existed in the peripheral vision field thanks to the pre-cue.

We focused on analyzing the driver's visual attention prior to negotiating blind corners. Because almost all the areas of the field of view were occupied as dead angle, as shown in Fig. 1, the peripheral vision may not always be important in predicting the PCHOs. Furthermore, all the participants focused on the blind areas across the central vision field before entering the corner, as shown in Fig. 7. We therefore concluded that although the simple visual condition for obstacles was used, the experiments retained their validity.

V. Conclusion

In this study, we attempted to establish the numerical safety criteria for PMVs while negotiating blind corners. We analyzed the driving behavior of a robotic PMV operated by a human driver. The PMV can measure the gaze of the driver, and localize its own pose. Using the PMV, we simulated the driver's visual attention and the PCHOs on a 3D map. The PCHOs are defined as obstacles that spring out from occluded areas with which a driver cannot avoid collision.

The participants of our experiments were one skillful (SD) and three non-skilled (NSD) drivers. The following deductions were made from the experimental results:

- Although the driving and eye-gaze behaviors of each driver were unique, similar PCHOs were observed in the results of both the SD and the NSDs.
- The relationship between the collision angle and linear velocity of the PCHOs revealed a boundary that divides expected and unexpected obstacles for drivers.

Our future research will include a more advanced attention analysis using an object classifier method, such as [44], and autonomous navigation in blind corners utilizing the safety criteria and its performance evaluation. Additionally, we plan to model the driving and eye-gaze behaviors, such as those presented in [45] to enable a more indepth comprehension of the human driving style.

Acknowledgment

This work was supported by the Nagoya-COI funded by the JST and JST-Mirai Program Grant Number JP-MJMI17C6, Japan. This work was also partially supported by KAKENHI 40786092 and Technova Inc.

References

[1] L. E. Kavraki, P. Svestka, Jean-Claude Latombe, and M. H. Overmars. Probabilistic roadmaps for path planning in high-dimensional configuration spaces. *IEEE Transactions Robotics and Automation*, 12(4):566–580, 1996.

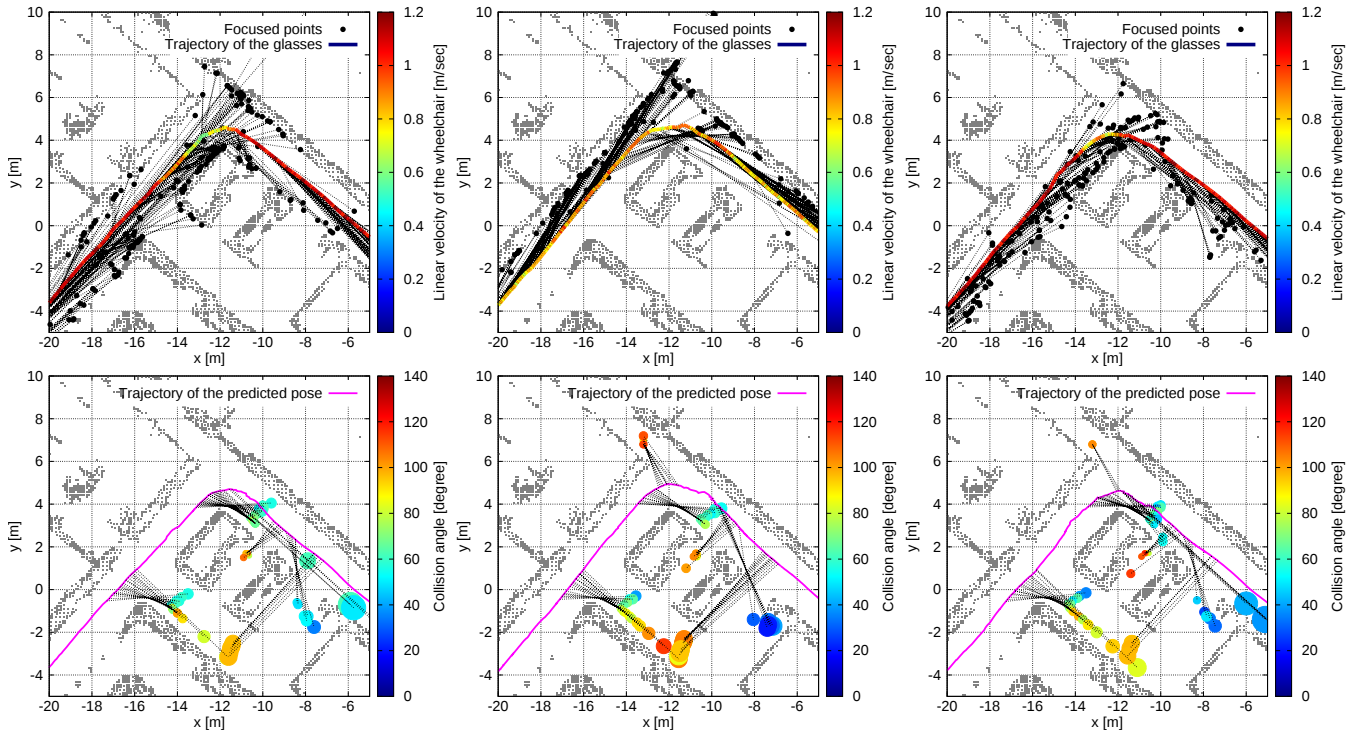

Fig. 8. Results of CW driving by the NSD1, NSD2, and NSD3 from the left

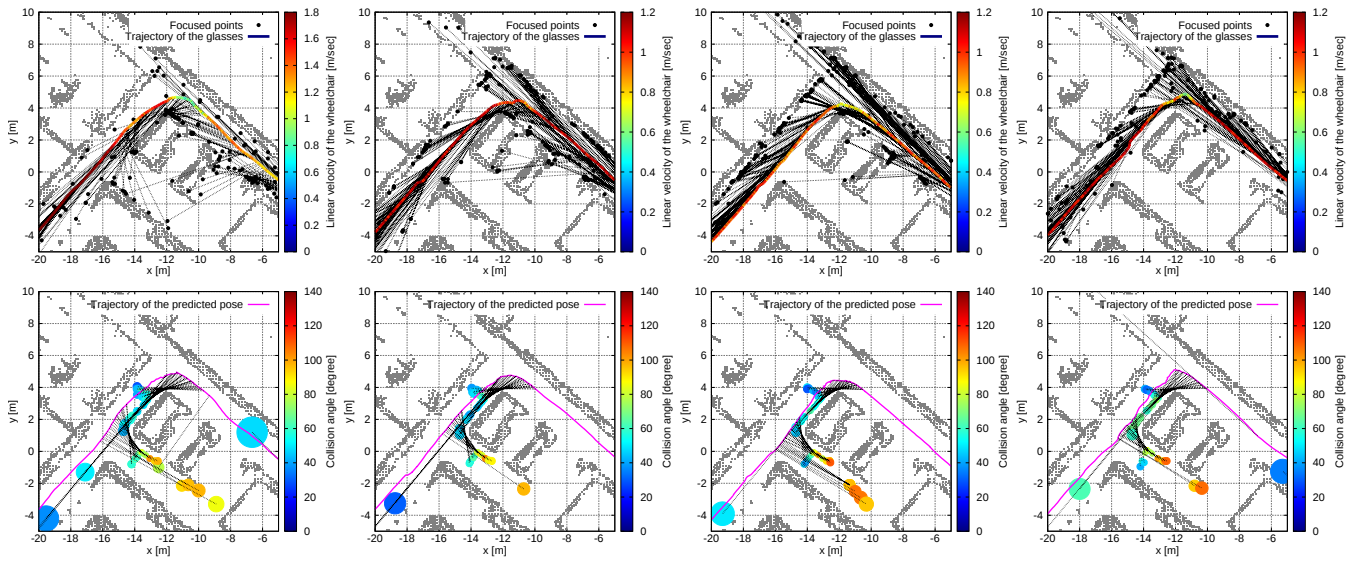

Fig. 9. Results of CCW driving by the SD, NSD1, NSD2, and NSD3 from the left.

[2] A. Koga, H. Okuda, Y. Tazaki, T. Suzuki, K. Haraguchi, and Z. Kang. Realization of different driving characteristics for autonomous vehicle by using model predictive control. In *Proceedings of the IEEE Intelligent Vehicles Symposium (IV)*, pages 722–728, 2016.

[3] L. Y. Morales, J. Even, N. Kallakuri, T. Ikeda, K. Shinozawa, T. Kondo, and N. Hagita. Visibility analysis for autonomous vehicle comfortable navigation. In *Proceedings of the IEEE International Conference on Robotics and Automation (ICRA)*, pages 2197–2202, 2014.

[4] T. Sawabe, K. Kanbara, N. Ukita, T. Ikeda, L. Y. Morales, A. Watanabe, and N. Hagita. Comfortable autonomous navigation based on collision prediction in blind occluded regions. In *Proceedings of the IEEE International Conference on Vehicular Electronics and Safety (ICVES)*, pages 87–92, 2015.

[5] T. Sawabe, M. Kanbara, and N. Hagita. Comfortable intelligence for evaluating passenger characteristics in autonomous wheelchairs. *IEICE TRANSACTIONS on Fundamentals of Electronics, Communications and Computer Sciences*, E101-A(9):1308–1316, 2018.

[6] E. Takeuchi, Y. Yoshihara, and N. Yoshiki. Blind area traffic prediction using high definition maps and LiDAR for safe driving assist. In *Proceedings of the IEEE International Conference on Intelligent Transportation Systems (ITSC)*, pages 2311–2316, 2015.

[7] M. Muffert, T. Milbich, D. Pfeiffer, and U. Franke. May I enter the roundabout? A time-to-contact computation based on stereo-vision. In *Proceedings of the IEEE Intelligent Vehicles Symposium (IV)*, pages 565–570, 2012.

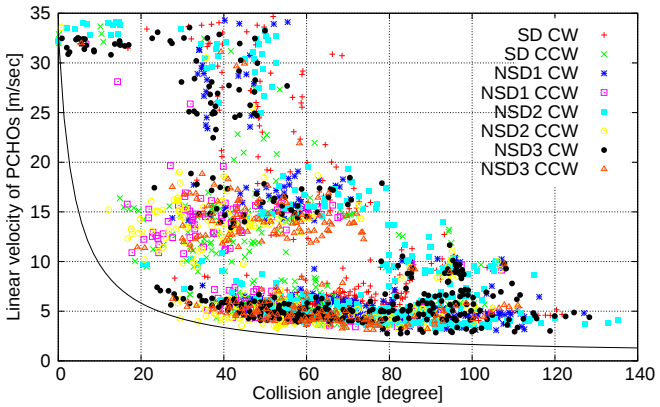

Fig. 10. Collision angle and linear velocity of the PCHOs.

[8] S. Hörmann, F. Kunz, D. Nuss, S. Reuter, and K. Dietmayer. Entering crossroads with blind corners. A safe strategy for autonomous vehicles. In *Proceedings of the IEEE Intelligent Vehicles Symposium (IV)*, pages 727–732, 2017.

[9] L. Y. Morales, Y. Yoshihara, N. Akai, E. Takeuchi, and Y. Ninomiya. Proactive driving modeling in blind intersections based on expert driver data. In *Proceedings of the IEEE Intelligent Vehicles Symposium (IV)*, pages 901–907, 2017.

[10] Y. Yoshihara, L. Y. Morales, N. Akai, E. Takeuchi, and Y. Ninomiya. Autonomous predictive driving for blind intersections. In *Proceedings of the IEEE/RSJ Intelligent Robots and Systems (IROS)*, pages 3452–3459, 2017.

[11] N. Akai, L. Y. Morales, E. Takeuchi, Y. Yoshihara, and Y. Ninomiya. Robust localization using 3D NDT scan matching with experimentally determined uncertainty and road marker matching. In *Proceedings of the IEEE Intelligent Vehicles Symposium (IV)*, pages 1357–1364, 2017.

[12] N. Akai, L. Y. Morales, T. Yamaguchi, E. Takeuchi, Y. Yoshihara, H. Okuda, T. Suzuki, and Y. Ninomiya. Autonomous driving based on accurate localization using multilayer LiDAR and dead reckoning. In *Proceedings of the IEEE International Conference on Intelligent Transportation Systems (ITSC)*, pages 1147–1152, 2017.

[13] M. Kuderer, S. Gulati, and W. Burgard. Learning driving styles for autonomous vehicles from demonstration. In *Proceedings of the IEEE International Conference on Robotics and Automation (ICRA)*, pages 2641–2646, 2015.

[14] C. Richter and N. Roy. Safe visual navigation via deep learning and novelty detection. In *Robotics: Science and Systems (RSS)*, 2017.

[15] L. Y. Morales, N. Akai, and H. Murase. Towards predictive driving through blind intersections. In *Proceedings of the IEEE International Conference on Intelligent Transportation Systems (ITSC)*, pages 716–722, 2018.

[16] K. Sama, L. Y. Morales, N. Akai, H. Liu, E. Takeuchi, and K. Takeda. Driving feature extraction and behavior classification using an autoencoder to reproduce the velocity styles of experts. In *Proceedings of the IEEE International Conference on Intelligent Transportation Systems (ITSC)*, pages 1337–1343, 2018.

[17] J. A. Michon. A critical view of driver behavior models: What do we know, what should we do? *Human Behavior and Traffic Safety*, pages 485–520, 1985.

[18] M. F. Land. Predictable eye-head coordination during driving. *Nature*, 359(6393):318–320, 1992.

[19] Q. Ji and X. Yang. Real-time eye, gaze, and face pose tracking for monitoring driver vigilance. *Real-Time Imaging*, 8:357–377, 2002.

[20] A. Tawari, K. H. Chen, and M. M. Trivedi. Where is the driver looking: Analysis of head, eye and iris for robust gaze zone estimation. In *Proceedings of the IEEE International Conference on Intelligent Transportation Systems (ITSC)*, pages 988–994, 2014.

[21] A. Doshi and M. Trivedi. Investigating the relationships between gaze patterns, dynamic vehicle surround analysis, and driver intentions. In *Proceedings of the IEEE Intelligent Vehicles Symposium (IV)*, pages 887–892, 2009.

[22] C. Miyajima, S. Yamazaki, T. Bando, K. Hitomi, H. Terai, H. Okuda, T. Hirayama, M. Egawa, T. Suzuki, and K. Takeda. Analyzing driver gaze behavior and consistency of decision making during automated driving. In *Proceedings of the IEEE Intelligent Vehicles Symposium (IV)*, pages 1293–1298, 2015.

[23] T. Hirayama, K. Mase, and K. Takeda. Analysis of temporal relationships between eye gaze and peripheral vehicle behavior for detecting driver distraction. *International Journal of Vehicular Technology*, 2013(285927), 2013.

[24] T. Hirayama, K. Mase, C. Miyajima, and K. Takeda. Classification of driver's neutral and cognitive distraction states based on peripheral vehicle behavior in driver's gaze transition. *IEEE Transactions on Intelligent Vehicles*, 1(2):148–157, 2016.

[25] L. Paletta, K. Santner, G. Fritz, H. Mayer, and J. Schrammel. 3D attention: Measurement of visual saliency using eye tracking glasses. In *CHI '13 Extended Abstracts on Human Factors in Computing Systems*, CHI EA '13, pages 199–204. ACM, 2013.

[26] H. Wang, J. Pi, T. Qin, S. Shen, and B. E. Shi. SLAM-based localization of 3D gaze using a mobile eye tracker. In *Proceedings of the 2018 ACM Symposium on Eye Tracking Research & Applications*, ETRA '18, pages 65:1–65:5. ACM, 2018.

[27] K. Pirker, M. Ruether, G. Schweighofer, and H. Bischof. GPSlam: Marrying sparse geometric and dense probabilistic visual mapping. In *British Machine Vision Conference*, 2011.

[28] H. Strasdat, A. J. Davison, J. M. M. Montiel, and K. Konolige. Double window optimisation for constant time visual SLAM. In *Proceedings of the IEEE International Conference on Computer Vision (ICCV)*, pages 2352–2359, 2011.

[29] N. Rhinehart and K. Kitani. First-person activity forecasting with online inverse reinforcement learning. In *Proceedings of the IEEE International Conference on Computer Vision (ICCV)*, pages 3696–3705, 2017.

[30] K. M. Kitani, B. D. Ziebart, J. A. Bagnell, and M. Hebert. Activity forecasting. In *European Conference on Computer Vision (ECCV)*, 2012.

[31] G. Grisetti, C. Stachniss, and W. Burgard. Improved techniques for grid mapping with Rao-Blackwellized particle filters. *IEEE Transaction on Robotics*, 23(1):34–46, 2007.

[32] A. Hornung, K. M. Wurm, M. Bennewitz, C. Stachniss, and W. Burgard. Octomap: An efficient probabilistic 3D mapping framework based on octrees. *Autonomous Robots*, 34(3):189–206, April 2013.

[33] N. Akai, L. Y. Morales, and H. Murase. Mobile robot localization considering class of sensor observations. In *Proceedings of the IEEE/RSJ Intelligent Robots and Systems (IROS)*, pages 3159–3166, 2018.

[34] D. B. Henson. *Visual Fields*. Oxford University Press, 1993.

[35] J. D. Rains. Signal luminance and position effects in human reaction time. *Vision Research*, 3:239–251, 1963.

[36] R. J. W. Mansfield. Latency functions in human vision. *Vision Research*, 13:2219–2234, 1973.

[37] J. M. Findlay and I. D. Gilchrist. *Active Vision*. Oxford University Press, 2003.

[38] M. Ikeda and T. Takeuchi. Influence of foveal load on the functional visual field. *Perception & Psychophysics*, 18(4):255–260, 1975.

[39] T. Miura. Coping with situational demands: A study of eye movements and peripheral vision performance. *Vision in Vehicles*, pages 205–216, 1986.

[40] T. Miura. Visual search in intersections: An underlying mechanism. *Journal of International Association of Traffic and Safety Sciences*, 16:42–49, 1992.

[41] C. Rogers, S. K. Rushton, and P. A. Warren. Peripheral visual cues contribute to the perception of object movement during self-movement. *i-Perception*, 2017.

[42] J. Rasmussen. Skills, rules, and knowledge; signals, signs, and symbols, and other distinctions in human performance models. *IEEE Transactions on Systems, Man, and Cybernetics*, 13(3):257–266, May 1983.

[43] M. Ishihara, K. Imanaka, and S. Mori. Lateralized effects of target location on reaction times when preparing for manual aiming at a visual target. *Human Movement Science*, 21:563–582, 2002.

[44] J. Redmon and A. Farhadi. YOLOv3: An incremental improvement. *CoRR*, abs/1804.02767, 2018.

[45] N. Akai, T. Hirayama, L. Y. Morales, Y. Akagi, H. Liu, and H. Murase. Driving behavior modeling based on hidden Markov models with driver's eye-gaze measurement and ego-vehicle localization. In *Proceedings of the IEEE Intelligent Vehicles Symposium (IV)*, pages 828–835, 2019.